Improving the semi-empirical modelling of a single-screw expander for small organic Rankine cycles

Antonio Giuffrida

Politecnico di Milano – Dipartimento di Energia, Via R. Lambruschini 4, 20156 Milano, Italy

The common semi-empirical modelling adopted for positive-displacement rotary expanders is revised in this paper. Paying particular attention to the leakage flow rates, the mechanical losses at the shaft and the ambient heat losses by the proposal of a more physically sound modelling, this paper aims at improving the performance simulation of a single-screw expander for which there exists a wide experimental cam-paign in literature. In detail, the mechanical losses are modelled with an approach consistent with the Stribeck's theory, whereas the contributions of both natural convection and radiation are taken into account for a proper modelling of the ambient heat losses.

After calibration and validation of the modelling procedure, based on experimental data of the expan-der operation with R245fa, mean absolute percentage errors of 0.69%, 1.77% and 0.33% as regards mass flow rate, electric power output and exhaust fluid temperature, respectively, are calculated. These errors are lower than the ones reported by other researchers, so the current simulations are more consistent with the experimental data.

Considering the higher reliability for a better performance simulation by the new modelling procedure, the model is finally used to study the behavior of the expander. In particular, attention is paid to the mass flow rate, the shaft and the electric power outputs, the expander efficiency, as well as the ambient heat losses, and to their relations with the operation parameters such as the degree of fluid superheat at the expander inlet, the fluid pressure at the expander inlet, the pressure ratio and the rotational speed.

Keywords:
Single-screw expander
Semi-empirical modelling
R245fa
Performance simulation
Expander efficiency
Organic Rankine cycle

1. Introduction

The organic Rankine cycle (ORC) is a well proven technology used to produce useful work or electricity from heat at low temperature from renewable energy sources, such as solar or geothermal, and from low-grade heat produced in an industrial process which cannot be recovered [1,2].

The performance of an organic Rankine cycle is strictly dependent on the conditions of the heat source and cold sink, on the proper selection of the working fluid to exploit the heat source and on the selection of the expander [3]. The production of useful work from an ORC system relies on the expander behavior. How-ever, it is challenging to find a device with efficient performance, especially at lower capacity ranges. Several researchers have sug-gested positive-displacement expanders as a suitable solution [4]. Although they are not a commercially ready technology, lots of prototypes are available as developed for the purpose of laboratory experiments by modifying a commercial machine for air compression or HVAC applications to make it run in reverse mode. In this field, significant researches have been conducted on scroll-type expanders, as detailed in a number of papers [5–12]. More recent

E-mail address: antonio.giuffrida@polimi.it

Published Journal Article available at: http://dx.doi.org/10.1016/j.apenergy.2017.02.015

Nomenclature

$a_{leak,0}$	coefficient for leakage area, m^2
$a_{leak,1}$	coefficient for leakage area, m^2 bar^{-1}
A	area, m^2
AU	heat transfer coefficient, W K^{-1}
b_{nc}	coefficient of heat losses for natural convection, W $K^{-1.25}$
b_{ra}	coefficient of heat losses for radiation, W K^{-4}
BVR	built-in volume ratio
c_{ht}	convection coefficient, W m^{-2} K^{-1}
c_p	specific heat at constant pressure, J kg^{-1} K^{-1}
D	hydraulic diameter, m
err	error
e_m, e_P, e_T	weights
f	friction coefficient
FF	filling factor
$f_{loss,0}$	coefficient for mechanical losses, m^3
$f_{loss,1}$	coefficient for mechanical losses, m^3 s bar
h	specific enthalpy, J kg^{-1}
HVAC	heating, ventilation, and air conditioning
K	geometric coefficient, $m^{1.8}$
L	length, m
mep	mean effective pressure, Pa
$\dot{m}$	mass flow rate, kg s^{-1}
MAPE	mean absolute percentage error
n_g	number of grooves in the screw rotor
N	rotational speed, rpm
Nu	Nusselt number
ORC	organic Rankine cycle
p	pressure, Pa
P	power, W
Pr	Prandtl number
PR	pressure ratio
$\dot{Q}$	heat transfer rate, W
Re	Reynolds number
s	specific entropy, J kg^{-1} K^{-1}
T	temperature, K
U	thermal transmittance, W m^{-2} K^{-1}
v	specific volume, m^3 kg^{-1}
V	volume, m^3
$V_{g,max}$	volume of the groove at the end of the adapted expansion process, m^3
w	velocity, m s^{-1}
z	number of points for model calibration
α	dimensionless coefficient
γ	isentropic exponent
η	efficiency
λ	thermal conductivity, W m^{-1} K^{-1}
μ	dynamic viscosity, Pa s
ρ	density, kg m^{-3}
τ	torque, N m

Subscripts

amb	ambient
crit	critical
el	electric
exp	experimental
gen	generator
grid	grid
in	inlet
inv	inverter
int	internal
is	isentropic
leak	leakage
load	load
loss	loss
mech	mechanical
oa	overall
out	outlet
sh	shaft
sim	simulated
sse	single-screw expander
sw	swept
vol	volumetric
w	envelope

is the interest in another positive-displacement expander, namely the single-screw machine [13–18], even though the initial concept goes back to 1960 [18]. As a matter of fact, its configuration has some advantages over the twin-screw architecture [19–22] such as balanced loading of the main screw rotor, higher volumetric efficiency, long working life, low vibrations and a simplified configuration. Based on these characteristics, ORC systems based on single-screw expanders have recently gained attention [23–25].

As anticipated, a number of studies in the literature is dedicated to characterize and model the performance of scroll- and screw-type expanders. In general, theoretical modelling is an effective tool for predicting and improving the performance of positive-displacement expanders. Mathematical models of expanders have been proposed by many researchers, based on the models of the corresponding compressor. Although the deterministic model is the most common, because of the complex geometry and internal transport mechanisms, empirical and semi-empirical models are often applied to describe the thermodynamic behavior of positive-displacement expanders. In particular, the semi-empirical model consists of a series of thermodynamic equations deduced from mass, energy and momentum conservations, where critical parameters are determined according to experimental data. The work formerly presented by Winandy et al. [26] for a scroll compressor was taken as the starting point of the modelling developed by Lemort et al. [27] for an open-drive scroll expander integrated in an ORC system. Such an expander model allows to investigate the variations of the expander performance with the system operating conditions. As shown in Fig. 1, supply pressure drop (0–1), heat transfer (1–2 and 5–6), internal leakage (2–4) and internal expansion (2–4) stages are included in the whole

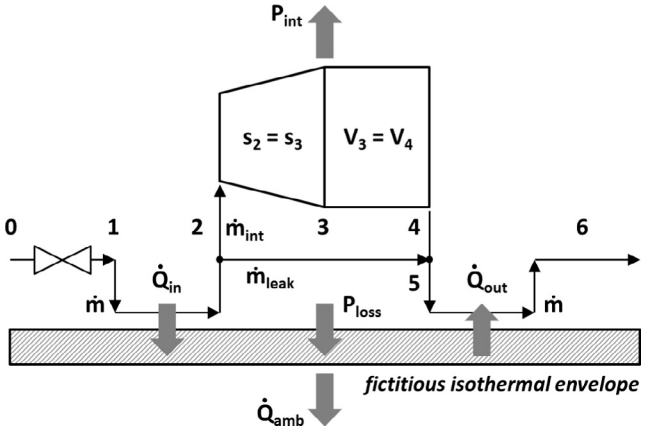

Fig. 1. Conceptual scheme of the semi-empirical model proposed for an open-drive scroll expander by Lemort et al. [27].

thermodynamic process. Evaluations of the mass flow rate, the shaft power and the exhaust temperature predicted by this model were compared with the experimental results of an open-drive scroll expander. The agreement between the measurement and the prediction by the model was very good, with maximum devia-tions of 2% for the mass flow rate and of 5% for the shaft power out-put. Based on this work, a semi-empirical model for hermetic scroll expanders was developed as well [28], by taking the electro-mechanical losses of the asynchronous generator into account. Other researchers have successfully adopted a similar semi-empirical modelling for their studies of scroll [10,29–31] as well as screw expanders [17,24,32].

The current study aims at revising the semi-empirical approach formerly proposed by Lemort et al. [27] for simulating the performance of a positive-displacement expander. In detail, focus is made on a single-screw expander by proposing more physically sound formulations for mechanical power losses as well as ambient heat losses, then the current model is calibrated and validated based on the experimental data reported by Desideri et al. [25]. Compared to the common semi-empirical approach, as adopted by Ziviani et al. [32], the current model results more reliable in simulating the performance of the expander.

2. The expander model

The semi-empirical model proposed by Lemort et al. [27] is the starting point for the current study. A description of the expansion process modelling, along with the related equations, is included in this section.

2.1. Processing of the working fluid

Fig. 1 shows the processing of the working fluid as it flows through the positive-displacement expander in a number of hypothetical stages, as described hereafter. Some assumptions are preliminarily introduced:

- the kinetic energy of the fluid is neglected in comparison with its internal energy,
- the fluid experiences no pressure drop at the outlet of the expander,
- fluid leakages through the clearances are assumed to be adiabatic,
- the presence of lubricating oil in a mixture with the working fluid is neglected.

The last assumption is justified according to the results achieved by the author in a previous work about the performance simulation of a family of twin-screw compressors [33]. As a matter of fact, absolutely acceptable results were achieved in the case of ignoring up to about 1.7 vol.% of oil in the refrigerant at the suction of the compres-sor (low pressure side), i.e. about 15 vol.% if considering the volu-metric flow rate at the delivery of the compressor (high pressure side).[1] These values are significantly greater than the ones character-istic of the single-screw expander to be modelled [25]. As anticipated by Melotte [34], oil is present in the cycle to lubricate the expander and its proportion is 3 L for 90 L of working fluid at the tank of the system, i.e. 3.23% of the total volume of fluid in the liquid phase.

2.1.1. Adiabatic supply pressure drop

This process ($0 \rightarrow 1$ in Fig. 1) accounts for the throttling at the expander inlet, during the filling of the variable volume chambers. An isentropic flow through a converging nozzle whose cross sectional area is A_{in} is introduced:

$$\dot{m} = \rho_{1,is} \cdot A_{in} \cdot \sqrt{2 \cdot (h_0 - h_{1,is})} \tag{1}$$

Because of the steady-state nature of the model, the area A_{in} stands for an average value of the inlet port cross-sectional area over the entire filling process. Based on Eq. (1), it is possible to calculate the pressure p_1 during the filling of the variable volume chambers, whereas h_1 is equal to h_0 owing to the throttling process.

2.1.2. Isobaric supply cooling-down

Heat transfer ($1 \rightarrow 2$ in Fig. 1) occurs between the fluid entering the variable volume chambers and a fictitious isothermal envelope, which is a specific lumped variable [27]. The supply heat transfer is modelled as:

$$\dot{Q}_{in} = \dot{m} \cdot (h_1 - h_2) = \left[1 - e^{-\frac{AU_{in}}{\dot{m} \cdot c_p}}\right] \cdot \dot{m} \cdot c_p \cdot (T_1 - T_w) \tag{2}$$

As regards the thermal transmittance in Eq. (2)

$$U = \frac{Nu \cdot \lambda}{L} \tag{3}$$

both the Nusselt number and the conductivity depend on the working fluid. The Nusselt number is here calculated according to the commonly used Dittus-Boelter correlation [35]:

$$Nu = 0.023 \cdot Re^{0.8} \cdot Pr^{m} \tag{4}$$

The exponent m is equal to 0.4 if the fluid is heated by the wall, otherwise it is equal to 0.3 (the fluid is cooled by the wall). Reynolds and Prandtl numbers are notoriously formulated as

$$Re = \frac{\rho \cdot w \cdot \mathrm{D}}{\mu} \tag{5}$$

$$Pr = \frac{c_p \cdot \mu}{\lambda} \tag{6}$$

Thus, the supply heat transfer coefficient AU_{in} is proportional to a relatively complex function

$$AU_{in} \propto \frac{\lambda}{L} \cdot Re^{0.8} \cdot Pr^{m} \tag{7}$$

which can be finally simplified as

$$AU_{in} = K_{in} \cdot \lambda \cdot \left(\frac{\dot{m}}{\mu}\right)^{0.8} \cdot Pr^{m} \tag{8}$$

where K_{in} is a geometric constant taking the area involved in the heat transfer into account.

This formulation is novel as common semi-empirical modelling just considers a heat transfer coefficient dependent on the only flow rate [26–28,32,36]. Here, in addition to the dependence on the mass flow rate, the supply heat transfer coefficient also depends on the thermo-physical properties of the working fluid.

2.1.3. Internal leakage

The mass flow rate entering the expander, as schematized in Fig. 1, is split into a first flow rate, necessary to cause the shaft to rotate at a specified rotational speed, which is related to the swept volume, and a second flow rate responsible for leakages:

$$\dot{m} = \rho_2 \cdot \frac{V_{sw}}{BVR} \cdot N + \dot{m}_{leak} \tag{9}$$

where V_{sw} represents the maximum displacement volume, at the end of the adapted expansion process, and BVR is the built-in volume ratio, as better shown in Fig. 2.

[1] The density of the (compressible) working fluid is obviously greater at higher pressures, resulting in an increase in the percentage fraction of the lubricating oil.

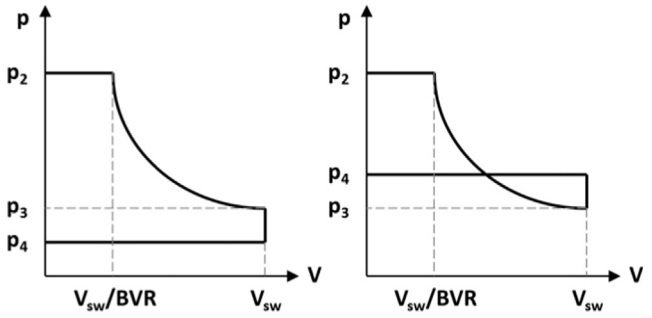

Fig. 2. Schematic under- and over-expansion processes in the p-V diagram (on the left and on the right, respectively).

No useful expansion is related to fluid leakages through the expander, so this phenomenon results in a significant loss. All leakage paths are lumped into a hypothetical area A_{leak}, which is used to simulate the leakage flow rate similarly as in Eq. (1):

$$\dot{m}_{leak} = \rho_{leak} \cdot A_{leak} \cdot \sqrt{2 \cdot (h_2 - h_{leak})} \tag{10}$$

i.e. the flow rate through an isentropic nozzle whose outlet area is A_{leak}. The pressure at the inlet of this fictitious nozzle is p_2, whereas the pressure at the outlet is the highest between p_4 (equal to the pressure at the expander outlet, $p_4 = p_5 = p_6$) and $p_{crit,leak}$:

$$p_{crit,leak} = p_2 \cdot \left(\frac{2}{\gamma + 1}\right)^{\frac{\gamma}{\gamma - 1}} \tag{11}$$

which is the critical pressure calculated from pressure p_2 by considering the working fluid as a perfect gas, with γ given by the ratio between the specific heat at constant pressure and the specific heat at constant volume [31]. Both ρ_{leak} and h_{leak} in Eq. (10) are calculated after the highest pressure between p_4 and $p_{crit,leak}$ is determined, along with the condition $s_{leak} = s_2$.

As regards the area A_{leak}, a constant value is usually adopted in semi-empirical modelling [27]. Nevertheless, a function depending on the expander load is here introduced:

$$A_{leak} = a_{leak,0} + a_{leak,1} \cdot p_{load} \tag{12}$$

where p_{load} is a pressure related to the expander load, as better detailed in the following. Thus, the second term in the right side of Eq. (12) stands for a spring-like contribution, which simulates clearances as load dependent. Eq. (12) revises the approach adopted elsewhere [28], where a similar formulation with the fluid pressure at the expander inlet instead of the here introduced p_{load} was used. Although the fluid processed by the expander is warmer than in a compressor [33], possible variations of the area A_{leak} due to thermal deformations are not taken into account.

2.1.4. Adiabatic expansion

The expansion process is divided into two stages, as shown in Fig. 1.

The first stage considers an isentropic expansion to the adapted pressure (2 → 3). The adapted pressure is related to the built-in volume ratio of the positive-displacement expander:

$$v_3 = BVR \cdot v_2 \tag{13}$$

Thus, the adapted conditions are determined by Eq. (13) and $s_3 = s_2$.

The second stage is an adiabatic expansion at constant machine volume (3 → 4). As schematized in Fig. 2, under- and over-expansion losses occur at this stage, when the adapted pressure is higher or lower, respectively, than the system pressure at the expander outlet. In order to equalize these pressures, the model assumes that some fluid flows out of or into the variable volume chambers instantaneously [27], after the chambers open on the outlet line and the fluid is no more trapped.

As formerly demonstrated by Lemort et al. [27], both under- and over-expansion at constant machine volume lead to the following relation:

$$h_3 - h_4 = v_3 \cdot (p_3 - p_4) \tag{14}$$

2.1.5. Adiabatic fluid mixing

The mass flow rate related to the shaft rotation ($\dot{m}_{int}$ in Fig. 1), i.e. the first term in the right side of Eq. (9), and the leakage flow rate mix altogether (4 → 5), resulting in a slight increase in specific enthalpy:

$$h_5 = \frac{(\dot{m} - \dot{m}_{leak}) \cdot h_4 + \dot{m}_{leak} \cdot h_2}{\dot{m}} \tag{15}$$

2.1.6. Isobaric exhaust heating-up or cooling-down

Heat is exchanged between the fluid exiting the expander and the fictitious isothermal envelope (5 → 6 in Fig. 1) and is modelled as in Section 2.1.2:

$$\dot{Q}_{out} = \dot{m} \cdot (h_5 - h_6) = \left[1 - e^{-\frac{AU_{out}}{\dot{m} \cdot c_p}}\right] \cdot \dot{m} \cdot c_p \cdot (T_5 - T_w) \tag{16}$$

Of course, a geometric constant K_{out} is introduced in this case for calculating AU_{out}. Depending on the difference between T_5 and T_w, $\dot{Q}_{out}$ can be directed from the fluid to the wall or viceversa ($\dot{Q}_{out}$ is negative if $T_5 < T_w$ and directed as in Fig. 1).

2.2. Heat losses

Positive-displacement expanders are not adiabatic machines, as heat losses can be significant. Ambient heat losses are always simulated by introducing a global heat transfer coefficient AU_{amb} [26–29,32,36]:

$$\dot{Q}_{amb} = AU_{amb} \cdot (T_w - T_{amb}) \tag{17}$$

This relation is revised in the current paper, based on the consideration that the heat transfer coefficient in natural convection can be formulated as [35]

$$c_{ht} \propto \left(\frac{T_w - T_{amb}}{L}\right)^{\frac{1}{4}} \tag{18}$$

and a radiation term should also be taken into account:

$$\dot{Q}_{amb} = b_{nc} \cdot (T_w - T_{amb})^{\frac{5}{4}} + b_{ra} \cdot (T_w^4 - T_{amb}^4) \tag{19}$$

This is another novelty of the current work. T_w is the temperature of the fictitious isothermal envelope schematized in Fig. 1 and already introduced in Eqs. (2) and (16), even though the hypothesis of one fictitious metal temperature is not very appropriate [37]. In order to improve the semi-empirical modelling, use of at least two fictitious isothermal walls could be made [38], but no case with more than one fictitious isothermal walls is reported in the literature.

2.3. Power losses and power output

After determining the thermodynamic states as described in Section 2.1, the internal expander power is calculated by taking both the mass flow rates $\dot{m}$ and $\dot{m}_{leak}$ into account:

$$P_{int} = (\dot{m} - \dot{m}_{leak}) \cdot (h_2 - h_4) \tag{20}$$

The shaft power output is calculated from this internal power, after subtracting the mechanical power losses.

Semi-empirical models reported in open literature usually simulate mechanical power losses by means of simple relations. In detail, Lemort et al. [27] introduced a constant friction torque multiplied by the rotational speed, or proposed a relation of shaft losses proportional to the internal power, by introducing a con-stant mechanical efficiency [28]. More recently, Ziviani et al. [32] introduced a combination of the above-mentioned functions as

$$P_{loss} = \alpha \cdot P_{int} + P_{loss,0} + 2 \cdot \pi \cdot \tau_{loss} \cdot \frac{N}{60} \tag{21}$$

where α, $P_{loss,0}$ and τ_{loss} are constants to be identified. Nevertheless, none of the proposed relations adopted by other researchers developing semi-empirical modelling procedures is used in this paper. As a matter of fact, in this author's opinion, all these relations do not properly simulate the friction loss process from a physical point of view.

Referring to internal combustion engines, the mean effective pressure is usually introduced as representative of the load [39], so the internal power in Eq. (20) is re-written as

$$P_{int} = mep \cdot V_{sw} \cdot N \tag{22}$$

Thus, based on (i) the mass flow rate through the expander, as reported in Eq. (9), (ii) the relation between the specific volumes v_2 and v_3 in Eq. (13) and (iii) the internal power as introduced with Eq. (20), the mean effective pressure is calculated as

$$mep = \rho_3 \cdot (h_2 - h_4) \tag{23}$$

Eq. (23) returns a relative pressure representative of the mean load of the expander. Adding this mean effective pressure to the pressure level at the exhaust of the expander results in a mean absolute pressure on the rotating parts, namely p_{load} as previously introduced in Eq. (12). By taking a mean contact surface into account and after introducing a friction coefficient and a velocity, obviously related to the rotational speed, it is possible to calculate the mechanical power losses as

$$P_{loss} \propto f \cdot (mep + p_6) \cdot N \tag{24}$$

Ultimately, in order to simulate a friction coefficient consistent with the Stribeck's curve [40], the mechanical power losses are simulated as

$$P_{loss} = \left[f_{loss,0} + f_{loss,1} \cdot \frac{N}{(mep + p_6)} \right] \cdot (mep + p_6) \cdot N \tag{25}$$

where the second term in the square brackets attempts to reproduce the independent variable of the Stribeck's curve, related to the velocity times the dynamic viscosity, divided by the load [40]. The terms inside the square brackets actually account for the pro-duct between a dimensionless friction coefficient and a volume. Eq. (25) for mechanical losses at the shaft is the most important novelty of the current modelling.

Thus, the shaft power output is calculated as

$$P_{sh} = P_{int} - P_{loss} \tag{26}$$

This mechanical power is firstly converted into electric power by a generator and secondly processed by a four-quadrant inverter prior to the injection of the final electric power into the grid [25]:

$$P_{el,gen} = \eta_{gen} \cdot P_{sh} \tag{27}$$

$$P_{el,grid} = \eta_{inv} \cdot P_{el,gen} \tag{28}$$

The relations used for the efficiency of both the electric generator and the inverter are the ones formerly reported by Melotte [34] and already included in the work by Ziviani et al. [32], so they are here omitted for the sake of brevity.

2.4. Overall power balance

The mechanical power losses are assumed to be injected directly into the envelope (see Fig. 1), along with the electric generator losses, so the temperature T_w is calculated based on the following balance:

$$P_{loss} + (1 - \eta_{gen}) \cdot P_{sh} + \dot{Q}_{in} - \dot{Q}_{amb} \pm \dot{Q}_{out} = 0 \tag{29}$$

where the correct sign of the last term is fixed according to the temperature difference between T_5 and T_w. Otherwise, the temperature T_w can be calculated by the simpler power balance of the expander plus the electric generator:

$$P_{el,gen} + \dot{Q}_{amb} = \dot{m} \cdot (h_0 - h_6) \tag{30}$$

Based on the last two equations, it is possible to arrive at an original formula for the shaft power output. Adding Eqs. (29) and (30) results in

$$P_{loss} + P_{sh} + \dot{Q}_{in} \pm \dot{Q}_{out} = \dot{m} \cdot (h_0 - h_6) \tag{31}$$

After introducing the mechanical efficiency of the expander as

$$\eta_{mech} = \frac{P_{sh}}{P_{int}} \tag{32}$$

the following formula can be obtained:

$$P_{sh} = \eta_{mecc} \cdot [\dot{m} \cdot (h_0 - h_6) - (\dot{Q}_{in} \pm \dot{Q}_{out})] \tag{33}$$

This relation for the shaft power output will be re-called in the following, for a better characterization of the expander performance.

3. The experimental campaign

The current paper, as anticipated, focuses on the single-screw expander investigated by Desideri et al. [25] who tested a small-scale ORC system for waste heat recovery with two separate working fluids (R245fa and SES36) under different working conditions, in order to prove the feasibility of using a single-screw expander. In detail, a single-screw compressor characterized by a nominal shaft power of 11 kW was converted to operate as an expander. The modifications included the replacement of the seals of the main shaft and side plates of the housing, the star-wheel bearings, as well as enlarging the discharge port (suction port in compressor mode). Reference to Desideri et al. [25] is made here for further specific details.

Forty-three and thirty-six steady-state points were collected in the cases of operation with R245fa and SES36, respectively, and used to characterize the performance of the positive-displacement expander, by data analysis with the CoolProp data-base [41] for the fluid thermodynamic and transport properties, as developed by Bell et al. [42].

Here, the data of their experimental campaign, included in their paper as supplementary data, are used for model calibration and validation. Based on the same data, Ziviani et al. [32] recently proposed their semi-empirical model, which is mainly based on the common modelling procedure available in open literature. Benchmarking to such a model [32] will test the level of reliability of the modelling procedure proposed in the current paper.

4. The calculation environment

The model presented in Section 2 has been implemented in the MATLAB environment, along with a set of data specific of the operation of the expander in terms of pressures, temperatures, rotational speeds, mass flow rates as well as electric power outputs, coming from the experimental campaign [25]. However, some

model equations need the fluid thermodynamic and transport properties. Similarly to a lot of literature works, use of the REFPROP database, as developed by the National Institute of Standards and Technology of the United States [43], has been made here.

In the following, the calibration and validation of the model and the next performance analysis are limited to the only case of the expander operation with R245fa. As a matter of fact, according to ORC literature, R245fa is much more frequently used than SES36. Besides, the last available version of REFPROP does not include the properties of SES36, and the reliability of the CoolProp database as regards this fluid is not sufficiently satisfactory, as reported in Appendix A.

5. Calibration and validation of the model

Before using the proposed modelling procedure as a tool for simulating the performance of the single-screw expander, a proper tuning of the model is necessary to determine the values of all the parameters introduced throughout the equations in Section 2. These parameters have been identified based on the minimization of a global error function of the predictions of mass flow rate, electric power output and exhaust temperature:

$$err = e_m \cdot \sqrt{\frac{1}{z} \cdot \sum \left(\frac{\dot{m}_{sim} - \dot{m}_{exp}}{\dot{m}_{exp}} \right)^2} + e_P \cdot \sqrt{\frac{1}{z} \cdot \sum \left(\frac{P_{el,grid,sim} - P_{el,grid,exp}}{P_{el,grid,exp}} \right)^2} + e_T \cdot \sqrt{\frac{1}{z} \cdot \sum \left(\frac{T_{6,sim} - T_{6,exp}}{max(T_{6,exp}) - min(T_{6,exp})} \right)^2} \quad (34)$$

where each summation extends over the z points chosen for tuning and e_m, e_P and e_T are three weights, which can be set at the same value [17,27,36] or diversified [24,32]. The minimization process has been carried out by using an optimization routine, available in MATLAB Optimization Toolbox and specifically dedicated to multivariable function minimization, giving particular care to the check that the final set of parameters leads to the global minimum of Eq. (34). As a common optimization problem, an initial value and a variation range are necessary for each parameter to be determined. Among the parameters, the volume displacement (in expander mode) and the built-in volume ratio are related one another. Introducing $V_{g,max}$ as the volume of the groove in the screw rotor at the end of the adapted expansion process, equal to 57.39 cm^3 [18], and n_g as the number of grooves in the screw rotor, the maximum volume displacement (in compressor mode) is calculated as:

$$V_{sw} = 2 \cdot n_g \cdot V_{g,max} \quad (35)$$

V_{sw} divided by the built-in volume ratio returns the volume displacement in expander mode, as included in Eq. (9) and shown in Fig. 2. Moreover, based on the assumption of equal geometries involved in the heat transfer at both intake and exhaust, just one value, valid for both the geometric constant parameters K_{in} and K_{out}, has been determined.

In particular, Eq. (34) has been adopted for successive optimizations with variable weights e_m, e_P and e_T from time to time, which have been stopped according to a 0.1% variation of the error between two consecutive optimizations. The calibration of the model has been carried out by including thirty-four among the forty-three points reported by Desideri et al. [25] and precisely the ones with a pressure ratio (PR) greater than 5. Thus, the remaining nine points with PR $\leq$ 5 have been dedicated to the next validation. Like Ziviani et al. [32], such a division reserves 80% of the total experimental points for the calibration and the remaining 20% for the validation. Ultimately, based on the values e_m, = 57, e_P = 19 and e_T = 1, the identified parameters for the model of the expander are listed in Table 1.

Figs. 3–5 show parity plots of mass flow rate, electric power output and exhaust fluid temperature, based on all the available data. The dash-dot lines bound a range of ±5% for the mass flow rate, ±10% for the electric power output and ±3 K for the exhaust fluid temperature. In particular, the maximum errors result in 1.85% for the mass flow rate, 5.89% for the electric power output and 1.81 K for the exhaust fluid temperature. Compared to the results achieved by other researchers with a semi-empirical

Table 1
Model parameters (operation with R245fa).

Parameter	Description	Value	Units
$a_{leak,0}$	Coefficient for leakage area	$17 \cdot 10^{-6}$	m^2
$a_{leak,1}$	Coefficient for leakage area	$0.76 \cdot 10^{-6}$	$m^2\ bar^{-1}$
A_{in}	Inlet port cross-sectional area	$92.94 \cdot 10^{-6}$	m^2
b_{nc}	Coefficient of heat losses for natural convection	1.32	$W\ K^{-1.25}$
b_{ra}	Coefficient of heat losses for radiation	$3.14 \cdot 10^{-8}$	$W\ K^{-4}$
BVR	Built-in volume ratio	6	–
$f_{loss,0}$	Coefficient for mechanical losses	$103.2 \cdot 10^{-6}$	m^3
$f_{loss,1}$	Coefficient for mechanical losses	$-3.03 \cdot 10^{-6}$	$m^3\ s\ bar$
K_{in}	Coefficient for heat transfer at expander inlet	1.12	$m^{1.8}$
K_{out}	Coefficient for heat transfer at expander outlet	1.12	$m^{1.8}$

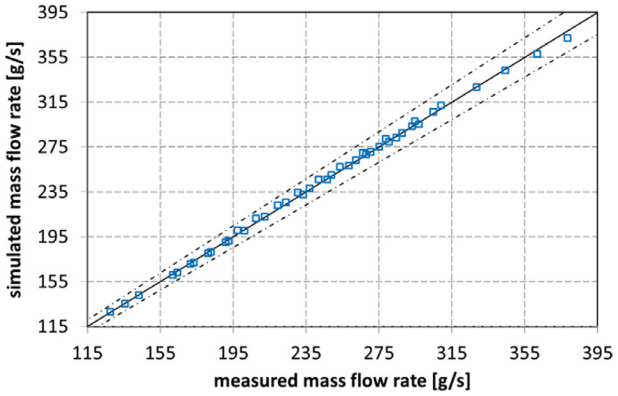

Fig. 3. Parity plot of mass flow rate (the dash-dot lines bound a range of ±5%).

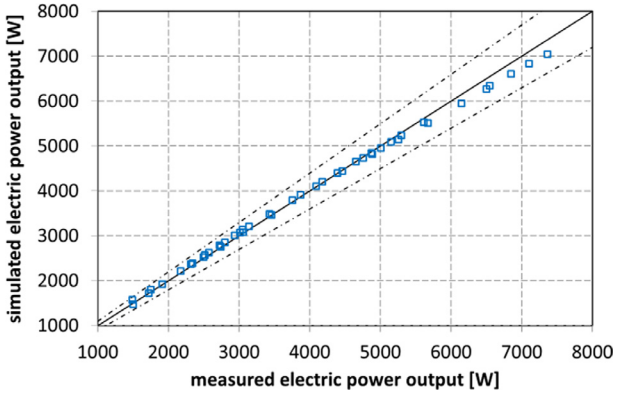

Fig. 4. Parity plot of electric power output (the dash-dot lines bound a range of ±10%).

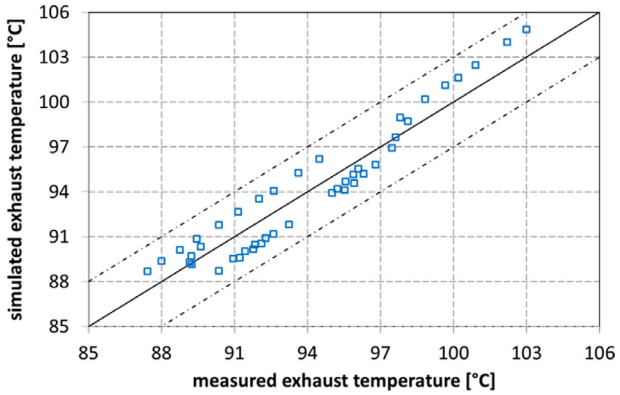

Fig. 5. Parity plot of exhaust fluid temperature (the dash-dot lines bound a range of ±3 K).

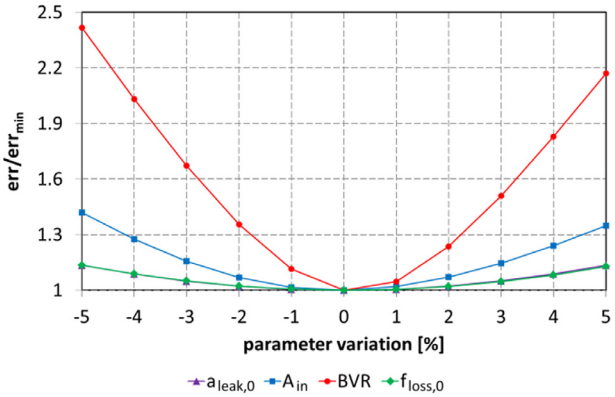

Fig. 6. Sensitivity of the result of Eq. (34) to the most significant model parameters.

Table 2
Comparison of mean absolute percentage error (MAPE).

	Current model (%)	Ziviani et al. [32] (%)
MAPE for mass flow rate	0.69	1.48
MAPE for electric power output	1.77	5.11
MAPE for exhaust fluid temperature	0.33	0.42

modelling approach,[2] this level of accuracy may be considered satisfying.

The results of the current model are even more appreciable when looking at the results in Table 2, where the mean absolute percentage errors are compared with the ones calculated by Ziviani et al. [32] with their model and the same experimental data. Although the parameters in Table 1 and the ones adopted by Ziviani et al. [32] for their model cannot be directly compared, as there are significant differences in some parts of two modelling approaches, the values in Table 2 point out that the current model improves considerably the state-of-the-art, as it is more reliable in performance simulation.

A sensitivity analysis has been made as well, by varying the identified parameters reported in Table 1 in a range from −5% to 5%. Fig. 6 shows the response of the model as the ratio err/err_{min} versus the variation of the actual parameter compared to the corresponding value in Table 1. In detail, err_{min} represents the minimum value reached by the function err in Eq. (34), which is obviously obtained when the error is calculated based on the parameters in Table 1. There is high sensitivity to the built-in volume ratio, related to the volume displacement in expander mode as previously anticipated, to the inlet port cross-sectional area and, in a lesser way, to the coefficients $a_{leak,0}$ and $f_{loss,0}$ for the leak-age area and the mechanical power losses, respectively (the effects are almost superimposed). The other parameters disturb very slightly the response of the model, so they are not shown in Fig. 6.

6. Performance analysis

Simulation results of the single-screw expander performance with R245fa are analyzed and discussed in this section. Along with the parameters found and reported in Table 1, the model requires the fluid inlet pressure and temperature, the pressure ratio (or the fluid outlet pressure) and the rotational speed as input variables in order to calculate the mass flow rate and the electric power to the grid, as primary outputs, as well as a number of secondary results (leakage flow rates, the shaft power output, ambient heat losses, etc.) as reported in Section 2.

A preliminary analysis is presented after setting two rotational speeds (2000 and 3000 rpm), three pressure levels of the fluid at the expander inlet (8, 10 and 12 bar), three pressure ratios for each pressure level of the fluid at the expander inlet (4, 5 and 6 in case of 8 and 10 bar and 5, 6 and 7 in case of 12 bar) and a degree of fluid superheat ranging from 5 K up to a maximum fluid temperature of 125 °C at the expander inlet.

Figs. 7–9 focus on results of mass flow rate, electric power output and ambient heat losses.

Fig. 7 shows that the higher the rotational speed the larger the flow rate. This trend, justified by Eq. (9), is consistent with the ones reported by Ayachi et al. [10] for a scroll expander, another positive-displacement machine. The larger mass flow rate in case of higher fluid pressure at the expander inlet is justified if one considers that a constant rotational speed is related to a constant volumetric flow rate and higher pressure brings about higher density. Fig. 7 also points out that the pressure ratio has no significant effect on the mass flow rate. As a matter of fact, the mass flow rate is just affected by the fluid conditions at the expander inlet, which are fixed as variable pressure ratios reflect on different pressures at the expander outlet.

Results of the electric power output as a function of the fluid temperature at the expander inlet are shown in Fig. 8, with reference to 12 bar of fluid pressure at the expander inlet, three pressure ratios and two rotational speeds. It is possible to appreciate that higher pressure ratio and rotational speed reflect on higher power output. Nevertheless, increasing the degree of fluid super-

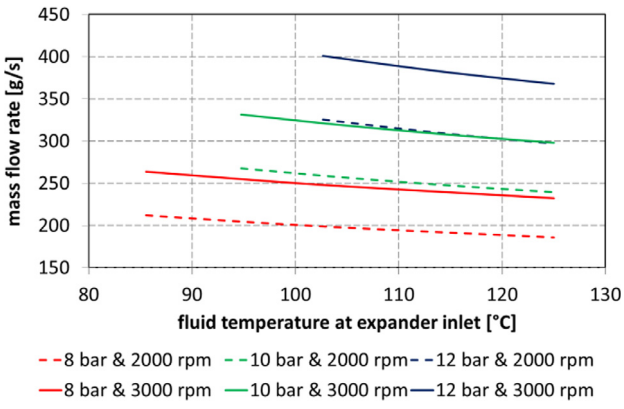

Fig. 7. Mass flow rate vs. fluid temperature at the expander inlet.

[2] As an example, the model proposed by Lemort et al. [28] for an hermetic scroll expander presented a maximum deviation between the prediction and the measurements of 2% for the mass flow rate, 6% for the shaft power, and 2 K for the exhaust temperature.

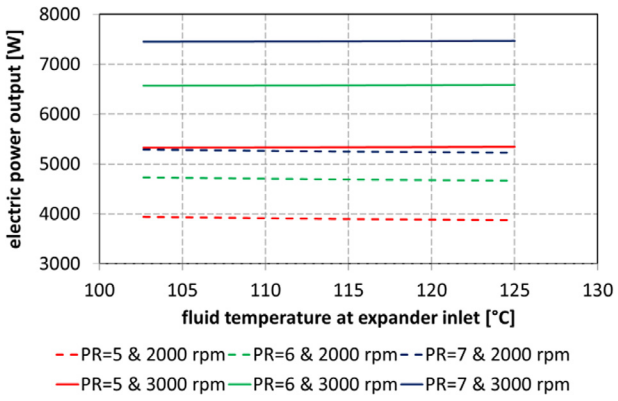

Fig. 8. Electric power output vs. fluid temperature at the expander inlet (fluid pressure at expander inlet equal to 12 bar).

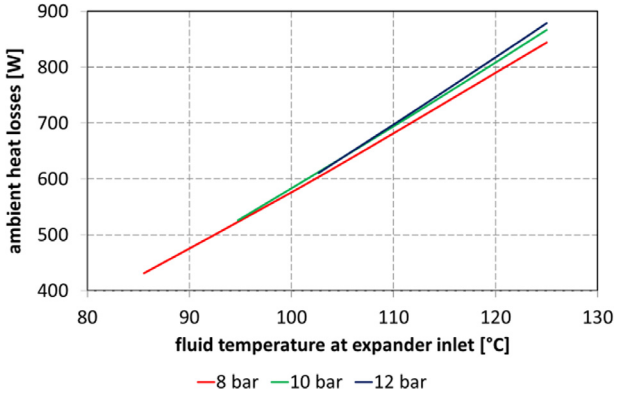

Fig. 9. Ambient heat losses vs. fluid temperature at the expander inlet for three fluid pressure levels at the expander inlet (pressure ratio and rotational speed equal to 6 and 3000 rpm).

heat does not bring about any significant improvement. The same constant trend of the electric power output is simulated for the mechanical power at the shaft, even though not reported for the sake of brevity.[3] Results with constant trend, similar to the one in Fig. 8, are calculated also in the cases of 8 and 10 bar of fluid pressure at the expander inlet, so increasing the fluid temperature beyond a certain value is fruitless from a power output point of view. In addition, the expander efficiency defined as:

$$\eta_{sse} = \frac{P_{sh}}{\dot{m} \cdot (h_0 - h_{6is})} \tag{36}$$

is calculated as slightly decreasing with the fluid temperature at the expander inlet (h_{6is} is calculated at the exhaust pressure with $s_{6is} = s_0$). Both a flat power output and a decreasing efficiency in case of higher degrees of fluid superheat at the expander inlet have been reported in a previous author' study on a scroll expander sim-ulated with a number of working fluids [31] and also pointed out by Yang et al. [44], based on their experimental activity on a scroll expander using R245fa. Furthermore, Declaye et al. [45] have high-lighted the dependence of the efficiency of an open-drive scroll expander on supply pressure, pressure ratio and rotational speed, but not on the fluid temperature at the expander inlet. Thus, the behavior in Fig. 8 is not unusual for positive-displacement expanders.

As far as can be ascertained that the power output is constant with the fluid temperature at the expander inlet, the heat losses increase in case of higher fluid temperature. Fig. 9 highlights a clear proportionality, with a modest dependence on the fluid pressure level at the expander inlet. Although not reported in Fig. 9, a really negligible reduction of the heat losses for a lower rotational speed (2000 rpm) and a slight reduction with the pressure ratio are calculated.

Based on these results, the degree of fluid superheat at the expander inlet should be limited as much as possible as (i) the power output does not seem to vary, (ii) the expander efficiency slightly reduces and (iii) the heat losses considerably increase. Thus, the degree of fluid superheat is fixed at 5 K in the next analysis.

Fig. 10 reports the relation between the mass flow rate and the fluid pressure at the expander inlet. Referring to a fixed exhaust pressure corresponding to 25 °C (around 1.5 bar), the mass flow rate seems to increase linearly with the fluid pressure. Considering that constant rotational speed requires constant volumetric flow rate, the trend in Fig. 10 could have been expected as the higher the pressure, the lower the specific volume. Such a trend is com-mon for positive-displacement expanders [46,47]. The greater slope with the shaft running at 3000 rpm than 2000 rpm can be simply justified by referring to Eq. (9). Fig. 10 also details the sim-ulated leakage flow rates, which increase with the fluid pressure and are larger at lower rotational speeds. As a matter of fact, the lower the flow rate (because of lower rotational speeds), the lower the pressure drop at the expander inlet, i.e. the higher the pressure $p_2 = p_1$. Based on Eqs. (10) and (11), the fictitious nozzle adopted for leakage simulation is critical, so the mass flow rate directly depends on the pressure p_2. Of course, the impact of leakages is more significant at 2000 rpm (around 30% of the entire mass flow rate) than at 3000 rpm (around 22% of the entire mass flow rate).

The volumetric performance of the expander is better represented by the filling factor, which is defined as the ratio between the actual mass flow rate and the mass flow rate theoretically displaced by the expander [27,28]:

$$FF = \frac{\dot{m}}{\rho_0 \cdot \frac{V_{sw}}{BVR} \cdot N} \tag{37}$$

The filling factor increases with internal leakage and supply cooling down, but decreases with the supply pressure drop. The evolution of the filling factor with the fluid pressure at the expander inlet for both 2000 and 3000 rpm is reported in Fig. 11, which also plots the volumetric efficiency defined as:

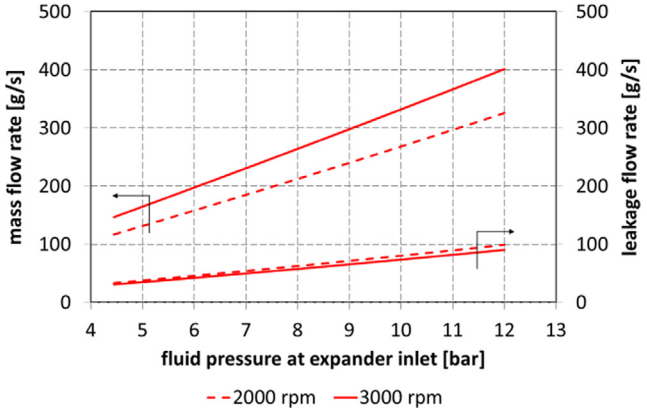

Fig. 10. Mass flow rate and leakage flow rate vs. fluid pressure at the expander inlet for two rotational speeds (the exhaust pressure is fixed and equal to the one corresponding to 25 °C).

[3] Of course, greater values for the shaft power output are calculated, owing to the efficiency of both generator and inverter.

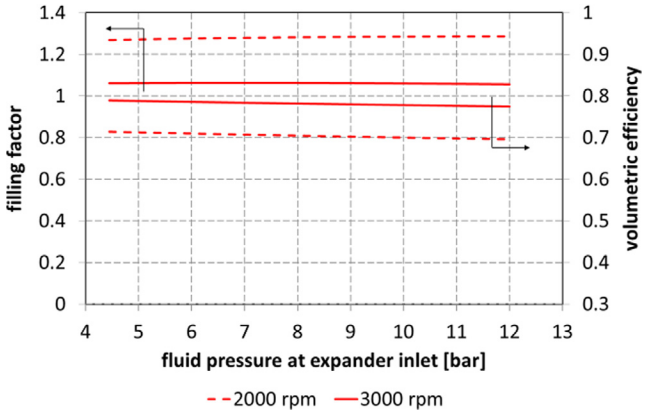

Fig. 11. Filling factor and volumetric efficiency vs. fluid pressure at the expander inlet for two rotational speeds (the exhaust pressure is fixed and equal to the one corresponding to 25 °C).

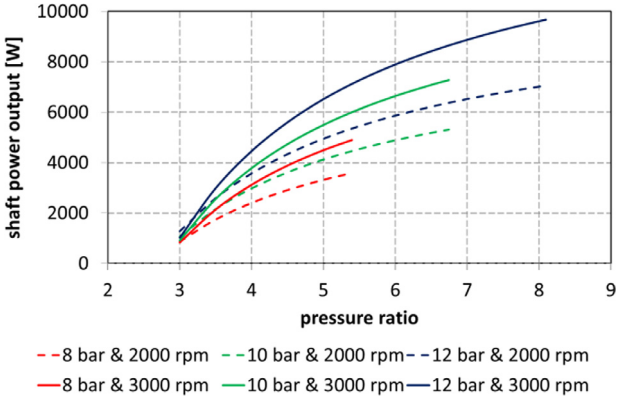

Fig. 12. Shaft power output vs. pressure ratio for three fluid pressure levels at the expander inlet and two rotational speeds.

$$\eta_{vol} = \frac{\dot{m}_{int}}{\dot{m}} = \frac{\dot{m} - \dot{m}_{leak}}{\dot{m}} \tag{38}$$

Both the filling factor and the volumetric efficiency are representative of the volumetric performance of the expander, even though different fluid densities are present in Eqs. (37) and (38), the latter implicitly including the fluid density ρ_2, as anticipated with Eq. (9).

A constant trend for the filling factor is calculated, fully consistent with the experimental data analysis by Ziviani et al. [32]. It can be observed that the lower the rotational speed, the higher the filling factor, due to the greater relative impact of the internal leakage, as previously anticipated. On the other hand, a slight reduction of the volumetric efficiency is calculated for higher fluid pressure at the expander inlet, because of the larger leakages.

Fig. 12 reports the results of performance simulations after setting three fluid pressure levels at the expander inlet and two rotational speeds. The highest pressure ratio for each curve is related to an exhaust pressure corresponding to 25 °C (around 1.5 bar). The shaft power output, which is a more representative result than the electric power output in terms of mechanical characterization of the expender, increases with (i) the fluid pressure at the expan-der inlet, (ii) the rotational speed and (iii) the pressure ratio. Sim-ilar trends were achieved by other researchers [10,45,48,49] in their characterization of scroll expanders. Thus, such a behavior is common for positive-displacement expanders.

The electric power output is shown in Fig. 13 and is lower than the mechanical power at the shaft, due to the losses at both the

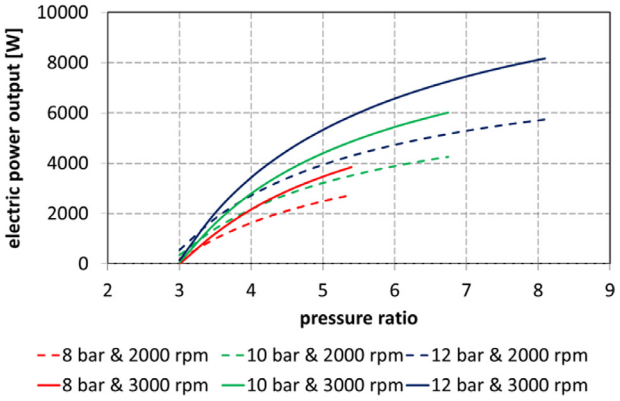

Fig. 13. Electric power output vs. pressure ratio for three fluid pressure levels at the expander inlet and two rotational speeds.

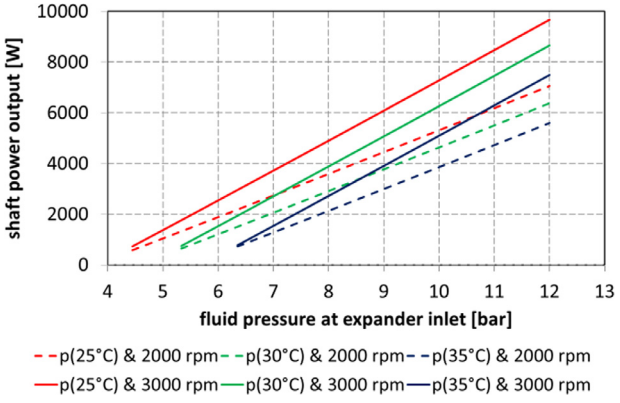

Fig. 14. Shaft power output vs. fluid pressure at the expander inlet for three pressure levels at the expander outlet and two rotational speeds.

electric generator and the inverter. However, the same trend as in Fig. 12 is calculated.

Differently from Fig. 12, Fig. 14 shows the mechanical power at the shaft as a function of the fluid pressure at the expander inlet, after setting the fluid pressure at the expander outlet and the rotational speed. The minimum fluid pressure for each curve in Fig. 14 is related to a pressure ratio of 3. In this case, it is possible to appreciate a linear trend with a greater slope in case of higher rotational speed. Of course, for a fixed fluid pressure at the expander inlet, the lower the pressure at the expander outlet, the higher the power output, which is fully consistent with the results in Fig. 12.

As anticipated with Eq. (36) and reported in Fig. 15, the expander efficiency is used as a figure of merit. Based on the calculations, it is an increasing monotonic function of the pressure ratio and seems to break the 60% barrier for the analyzed expander. Higher efficiency is possible for higher rotational speeds, when the weight of leakages is lower. Slight improvements in expander efficiency are calculated in case of lower fluid pressure at the expander inlet. In order to better understand this result, the mechanical efficiency as introduced with Eq. (32) is shown in Fig. 16. As a matter of fact, the mechanical efficiency is included in Eq. (33), so it directly affects both the shaft power output and the expander efficiency.

Other responses of the model that are worth of attention are the exhaust fluid temperature and the ambient heat losses, which are strictly related. Once again, the highest pressure ratio for each curve in Figs. 17 and 18 is related to an exhaust pressure corresponding to 25 °C (around 1.5 bar). The exhaust fluid temperature in Fig. 17 reduces when increasing the pressure ratio. This result is

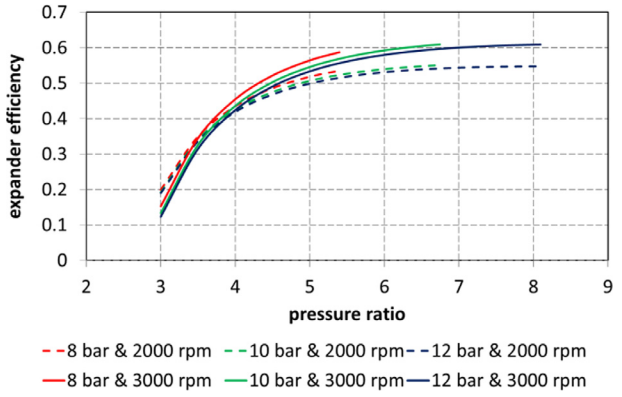

Fig. 15. Expander efficiency vs. pressure ratio for three fluid pressure levels at the expander inlet and two rotational speeds.

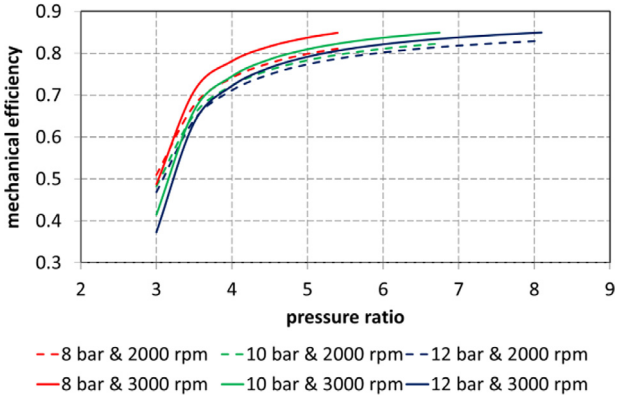

Fig. 16. Mechanical efficiency vs. pressure ratio for three fluid pressure levels at the expander inlet and two rotational speeds.

consistent with the fixed inlet conditions. Considering that simulations return a fictitious temperature T_w intermediate between the temperatures at the inlet and the outlet of the expander, the trends in Fig. 18 are justified. As shown in both Figs. 17 and 18, the effects of the fluid pressure at the expander inlet are evident, as formerly anticipated in Fig. 9, but the rotational speed affects slightly the trend. On the other hand, referring to the specific heat losses, i.e. the ambient heat losses divided by the mass flow rate, Fig. 19 shows that higher rotational speed causes lower specific heat losses, as expected, once the operating conditions are fixed.

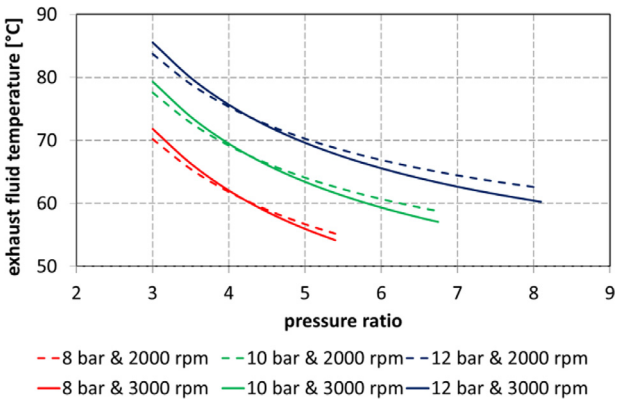

Fig. 17. Exhaust fluid temperature vs. pressure ratio for three fluid pressure levels at the expander inlet and two rotational speeds.

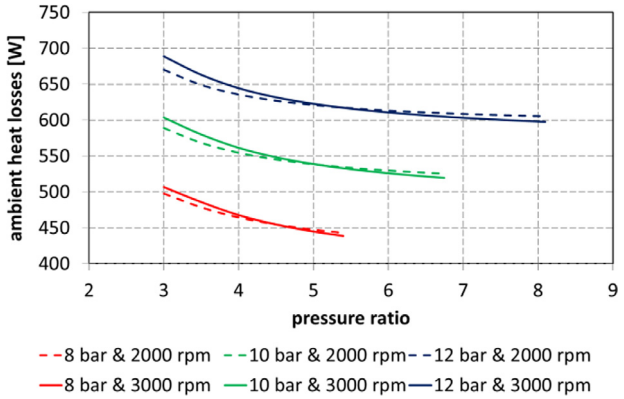

Fig. 18. Ambient heat losses vs. pressure ratio for three fluid pressure levels at the expander inlet and two rotational speeds.

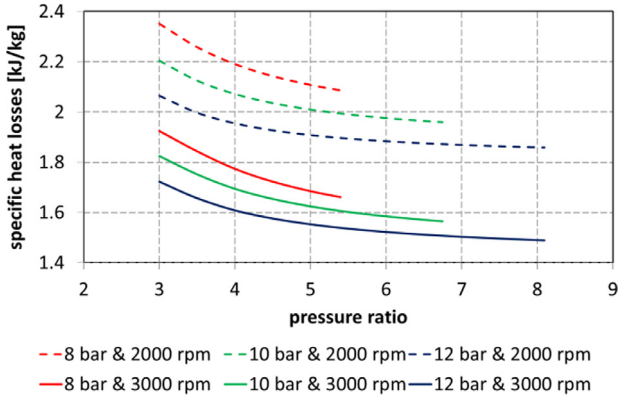

Fig. 19. Specific heat losses vs. pressure ratio for three fluid pressure levels at the expander inlet and two rotational speeds.

Ultimately, attention is paid to the ratio between ambient heat losses and shaft power output in order to point up the incidence of the former on mechanical power generation. Results in Fig. 20 suggest an almost negligible influence of the fluid pressure at the expander inlet, even though some differences can be appreciated in case of different rotational speeds. The heat losses are absolutely comparable with the shaft power output for very low pressure ratios, but the ratio reduces sharply for pressure ratios from 3 to around 3.5, then more moderately. In detail, the ratio between

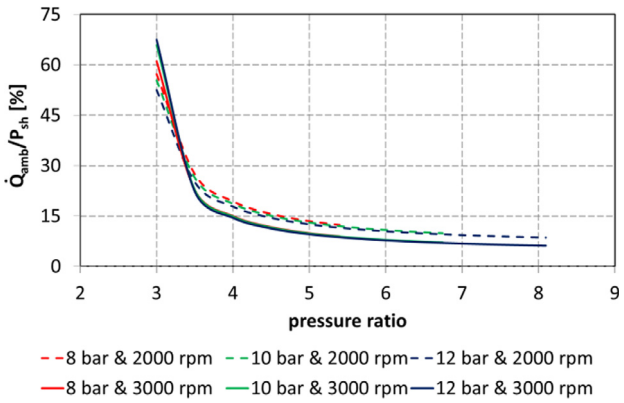

Fig. 20. Ratio between ambient heat losses and shaft power output vs. pressure ratio for three fluid pressure levels at the expander inlet and two rotational speeds.

ambient heat losses and shaft power output is calculated lower than 10% for pressure ratios greater than around 5 and 6.5, in case of rotational speed equal to 3000 and 2000 rpm, respectively. Of course, the trends in Fig. 20 refer to simulations based on 5 K of fluid superheat at the expander inlet. In case of higher fluid superheat, the incidence of ambient heat losses on mechanical power generation is more significant, according to the results presented in Figs. 8 and 9.

7. Conclusions

This paper has revised the common semi-empirical modelling for positive-displacement rotary expanders widely adopted in literature, with particular attention paid to the mechanical losses at the shaft and the ambient heat losses. Application of the proposed modelling to a single-screw expander has resulted in mean absolute percentage errors of 0.69%, 1.77% and 0.33% as regards mass flow rate, electric power output and exhaust fluid temperature, respectively. These errors are lower than the ones reported by other researchers [32], so the better performance simulation demonstrates the higher reliability of the proposed modelling.

The model has been later used to study the expander performance with the following main results.

- The mass flow rate for a fixed rotational speed increases with the fluid pressure at the expander inlet and decreases with high degrees of fluid superheat. The higher the rotational speed, the higher the mass flow rate.
- Once fixed the fluid pressure at the expander inlet, the pressure ratio and the rotational speed, the degree of fluid superheat at the expander inlet does not seem to affect the power output, which is almost constant. On the other hand, for fixed fluid pressure at the expander inlet and rotational speed, the higher the pressure ratio, the higher the power output. In addition, the higher the rotational speed, the higher the power output.
- The expander efficiency improves for higher pressure ratios, with the highest values achieved in case of higher rotational speed. The mechanical efficiency sensibly affects both the expander efficiency and the power output. In particular, a novel relation for the shaft power output dependent on the mechanical efficiency, the mass flow rate, the fluid enthalpies and the heat transfer rates at both inlet and outlet of the expander has been determined.
- The heat losses to the environment increase with the degree of fluid superheat at the expander inlet and reduce with the pressure ratio in the case of fixed fluid inlet conditions. Slight variations are calculated in case of different rotational speeds. The ratio between heat losses and shaft power output is significant for low pressure ratios, but it reduces sharply for pressure ratios from 3 to around 3.5, then more moderately.

Appendix A

As anticipated in Section 4, some model equations need the fluid thermodynamic and transport properties, calculated by means of REFPROP, even though the CoolProp database was chosen by Desideri et al. [25] for their data analysis.

Preliminarily, use of both the databases has been made in order to choose the most reliable library. In detail, the overall heat losses have been calculated by the general power balance:

$$P_{el,grid} + \dot{Q}_{amb,oa} = \dot{m} \cdot (h_0 - h_6) \quad \text{(A1)}$$

differently from Eq. (30) as, in this case, the overall heat losses include also the power dissipations of the inverter.

However, if slight differences in case of operation with R245fa have been calculated when using CoolProp instead of REFPROP, some points with negative overall heat losses in case of operation with SES36 have been calculated when using the CoolProp library (the last available version of REFPROP does not include the properties of SES36). This result cannot be accepted and suspicions are aroused on the reliability of the database as far as SES36 properties are concerned [50]. Thus, the overall heat losses in Eq. (A1) have been re-calculated after determining the enthalpies by means of the SOLKANE® Refrigerant software [51], resulting in no negative result for all the overall heat losses in Eq. (A1).

Figs. A1–A4 show comparisons of properties calculated by using CoolProp and SOLKANE® for three pressure levels in the superheated zone of SES36 up to 125 °C (the maximum fluid temperature according to the experimental data [25]). Although the fluid density is appreciably calculated by CoolProp, differences are evident in case of enthalpy, entropy, as well as specific heat at constant pressure, and point out the poor reliability of the CoolProp database for this fluid. Thus, as no communication can be set between MATLAB and SOLKANE®, the calibration and validation of the model is limited in Section 5 to the only case of the expander operation with R245fa.

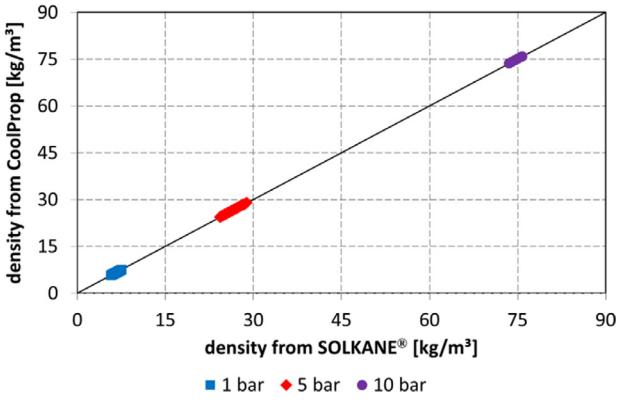

Fig. A1. Comparison of densities of SES36 for three pressure levels in the superheated zone up to 125 °C, as calculated by using CoolProp and SOLKANE®.

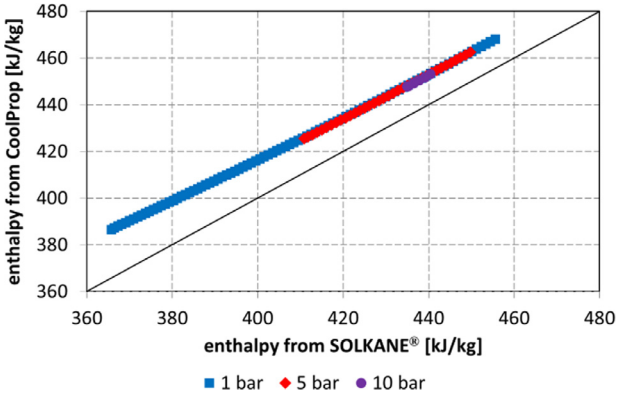

Fig. A2. Comparison of enthalpies of SES36 for three pressure levels in the superheated zone up to 125 °C, as calculated by using CoolProp and SOLKANE®.

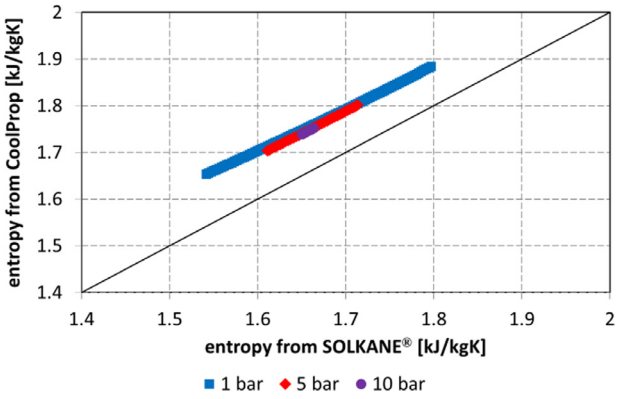

Fig. A3. Comparison of entropies of SES36 for three pressure levels in the super-heated zone up to 125 °C, as calculated by using CoolProp and SOLKANE®.

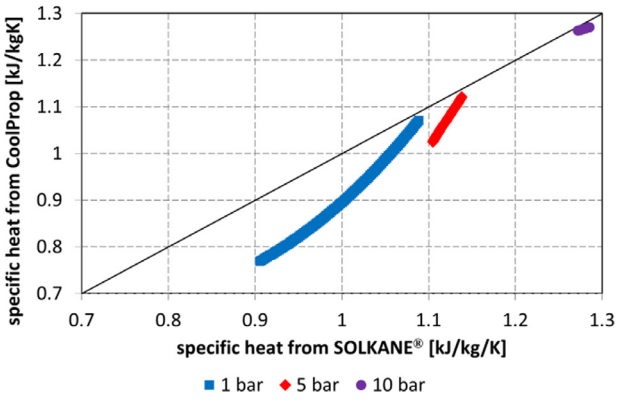

Fig. A4. Comparison of specific heats at constant pressure of SES36 for three pressure levels in the super-heated zone up to 125 ° C, as calculated by using CoolProp and SOLKANE®.

Appendix B. Supplementary material

Supplementary data [25] associated with this article can be found, in the online version, at http://dx.doi.org/10.1016/j.apenergy.2017.02.015.

References

[1] Quoilin S, van den Broek M, Declaye S, Dewallef P, Lemort V. Techno-economic survey of organic Rankine cycle ORC systems. Renew Sustain Energy Rev 2013;22:168–86.

[2] Colonna P, Casati E, Trapp C, Mathijssen T, Larjola J, Turunen-Saaresti T, et al. Organic Rankine cycle power systems: from the concept to current technology, applications, and an outlook to the future. J Eng Gas Turbines Power 2015;137 (10):100801.

[3] Bao J, Zhao L. A review of working fluid and expander selections for organic rankine cycle. Renew Sustain Energy Rev 2013;24:325–42.

[4] Imran M, Usman M, Park BS, Lee DH. Volumetric expanders for low grade heat and waste heat recovery applications. Renew Sustain Energy Rev 2016;57:1090–109.

[5] Quoilin S, Lemort V, Lebrun J. Experimental study and modeling of an Organic Rankine Cycle using scroll expander. Appl Energy 2010;87(4):1260–8.

[6] Clemente S, Micheli D, Reini M, Taccani R. Energy efficiency analysis of Organic Rankine Cycles with scroll expanders for cogenerative applications. Appl Energy 2012;97:792–801.

[7] Ibarra M, Rovira A, Alarcón-Padilla DC, Blanco J. Performance of a 5 kWe organic Rankine cycle at part-load operation. Appl Energy 2014;120:147–58.

[8] Song P, Wei M, Liu Z, Zhao B. Effects of suction port arrangements on a scroll expander for a small scale ORC system based on CFD approach. Appl Energy 2015;150:274–85.

[9] Chang JC, Hung TC, He YL, Zhang W. Experimental study on low-temperature organic Rankine cycle utilizing scroll type expander. Appl Energy 2015;155:150–9.

[10] Ayachi F, Ksayer EB, Neveu P, Zoughaib A. Experimental investigation and modeling of a hermetic scroll expander. Appl Energy 2016;181:256–67.

[11] Mendoza LC, Lemofouet S, Schiffmann J. Testing and modelling of a novel oil-free co-rotating scroll machine with water injection. Appl Energy 2017;185 (1):201–13.

[12] Ma Z, Bao H, Roskilly AP. Dynamic modelling and experimental validation of scroll expander for small scale power generation system. Appl Energy 2017;186(3):262–81.

[13] Wang W, Wu YT, Ma CF, Liu LD, Yu J. Preliminary experimental study of single screw expander prototype. Appl Therm Eng 2011;31(17–18):3684–8.

[14] He W, Wu Y, Peng Y, Zhang Y, Ma C, Ma G. Influence of intake pressure on the performance of single screw expander working with compressed air. Appl Therm Eng 2013;51(1–2):662–9.

[15] Wang W, Wu YT, Ma CF, Xia GD, Wang JF. Experimental study on the performance of single screw expanders by gap adjustment. Energy 2013;62:379–84.

[16] Xia GD, Zhang YQ, Wu YT, Ma CF, Ji WN, Liu SW, et al. Experimental study on the performance of single-screw expander with different inlet vapor dryness. Appl Therm Eng 2015;87:34–40.

[17] Ziviani D, Desideri A, Lemort V, De Paepe M, Van Den Broek M. Low-order models of a single-screw expander for organic Rankine cycle applications. IOP Conf Ser: Mater Sci Eng 2015;90(1):012061.

[18] Ziviani D, Bell IH, De Paepe M, Van Den Broek M. Update on single-screw expander geometry model integrated into an open-source simulation tool. IOP Conf Ser: Mater Sci Eng 2015;90(1):012064.

[19] Smith IK, Stosic N, Aldis CA. Development of the trilateral flash cycle system. Part 3: The design of high-efficiency two-phase screw expanders. Proc Instit Mech Eng, Part A: J Power Energy 1996;210(1):75–92.

[20] Öhman H, Lundqvist P. Experimental investigation of a Lysholm Turbine operating with superheated, saturated and 2-phase inlet conditions. Appl Therm Eng 2013;50(1):1211–8.

[21] Astolfi M. Techno-economic Optimization of Low Temperature CSP Systems Based on ORC with Screw Expanders. Energy Procedia 2015;69:1100–12.

[22] Read M, Smith I, Stosic N, Kovacevic A. Comparison of organic Rankine cycle systems under varying conditions using turbine and twin-screw expanders. Energies 2016;9(8):614.

[23] Zhang YQ, Wu YT, Xia GD, Ma CF, Ji WN, Liu SW, et al. Development and experimental study on organic Rankine cycle system with single-screw expander for waste heat recovery from exhaust of diesel engine. Energy 2014;77:499–508.

[24] Ziviani D, Woodland BJ, Georges E, Groll EA, Braun JE, Horton WT, et al. Development and a validation of a charge sensitive organic Rankine cycle (ORC) simulation tool. Energies 2016;9(6):389.

[25] Desideri A, Gusev S, Van den Broek M, Lemort V, Quoilin S. Experimental comparison of organic fluids for low temperature ORC (organic Rankine cycle) systems for waste heat recovery applications. Energy 2016;97:460–9.

[26] Winandy E, Saavedra CO, Lebrun J. Experimental analysis and simplified modelling of a hermetic scroll refrigeration compressor. Appl Therm Eng 2002;22(2):107–20.

[27] Lemort V, Quoilin S, Cuevas C, Lebrun J. Testing and modeling a scroll expander integrated into an organic Rankine cycle. Appl Therm Eng 2009;29:3094–102.

[28] Lemort V, Declaye S, Quoilin S. Experimental characterization of a hermetic scroll expander for use in a micro-scale Rankine cycle. Proc IMechE Part A: J Power Energy 2012;226:126–36.

[29] Twomey B, Jacobs PA, Gurgenci H. Dynamic performance estimation of small-scale solar cogeneration with an organic Rankine cycle using a scroll expander. Appl Therm Eng 2013;51:1307–16.

[30] Mendoza LC, Navarro-Esbrí J, Bruno JC, Lemort V, Coronas A. Characterization and modeling of a scroll expander with air and ammonia as working fluid. Appl Therm Eng 2014;70(1):630–40.

[31] Giuffrida A. Modelling the performance of a scroll expander for small organic Rankine cycles when changing the working fluid. Appl Therm Eng 2014;70 (1):1040–9.

[32] Ziviani D, Gusev S, Lecompte S, Groll EA, Braun JE, Horton WT, et al. Characterizing the performance of a single-screw expander in a small-scale organic Rankine cycle for waste heat recovery. Appl Energy 2016;181:155–70.

[33] Giuffrida A. A semi-empirical method for assessing the performance of an open-drive screw refrigeration compressor. Appl Therm Eng 2016;93:813–23.

[34] Melotte N. Experimental study and dynamic modeling of a Waste Heat Recovery Organic Rankine Cycle Master's thesis. Belgium: University of Liege; 2012.

[35] Incropera FP, De Witt PD, Bergman TL, Lavine AS. Introduction to heat transfer. 5th ed. John Wiley & Sons; 2007.

[36] Dardenne L, Fraccari E, Maggioni A, Molinaroli L, Proserpio L, Winandy E. Semi empirical modeling of a variable speed scroll compressor with vapor injection. Int J Refrig 2015;54:76–87.

[37] Stosic N. On heat transfer in screw compressors. Int J Heat Fluid Flow 2015;51:285–97.

[38] Cuevas C, Lebrun J, Lemort V, Winandy E. Characterization of a scroll compressor under extended operating conditions. Appl Therm Eng 2010;30 (6–7):605–15.

[39] Sen AK, Zheng J, Huang Z. Dynamics of cycle-to-cycle variations in a natural gas direct-injection spark-ignition engine. Appl Energy 2011;88 (7):2324–34.
[40] Lu X, Khonsari MM, Gelinck ERM. The Stribeck curve: experimental results and theoretical prediction. J Tribol 2006;128(4):789–94.
[41] www.coolprop.org [access 10.12.16].
[42] Bell IH, Wronski J, Quoilin S, Lemort V. Pure and pseudo-pure fluid thermophysical property evaluation and the open-source thermophysical property library CoolProp. Ind Eng Chem Res 2014;53(6):2498–508.
[43] www.nist.gov/srd/nist23.cfm [access 10.12.16].
[44] Yang SC, Hung TC, Feng YQ, Wu CJ, Wong KW, Huang KC. Experimental investigation on a 3 kW organic Rankine cycle for low grade waste heat under different operation parameters. Appl Therm Eng 2017;113:756–64.
[45] Declaye S, Quoilin S, Guillaume L, Lemort V. Experimental study on an open-drive scroll expander integrated into an ORC (Organic Rankine Cycle) system with R245fa as working fluid. Energy 2013;55:173–83.
[46] Miao Z, Xu J, Yang X, Zou J. Operation and performance of a low temperature organic Rankine cycle. Appl Therm Eng 2015;75:1065–75.
[47] Yang X, Xu J, Miao Z, Zou J, Yu C. Operation of an organic Rankine cycle dependent on pumping Flow rates and expander torques. Energy 2015;90:864–78.
[48] Muhammad U, Imran M, Lee DH, Park BS. Design and experimental investigation of a 1 kW organic Rankine cycle system using R245fa as working fluid for low-grade waste heat recovery from steam. Energy Convers Manage 2015;103:1089–100.
[49] Zhu J, Chen Z, Huang H, Yan Y. Effect of resistive load on the performance of an organic Rankine cycle with a scroll expander. Energy 2016;95:21–8.
[50] Thol M, Lemmon EW, Span R. Equation of state for a refrigerant mixture of R365mfc (1,1,1,3,3-Pentafluorobutane) and Galden HT 55 (Perfluoropolyether). Unpublished, 2012 - <http://www.coolprop.org/fluid_ properties/fluids/SES36.html> [access 29.01.17].
[51] Solvay Fluor GmbH. SOLKANE® Refrigerant Software 8.0.0.15.